Proceedings of the WORKSHOP on
Fundamental Issues and Future Research Directions for Parallel Mechanisms and Manipulators
October 3–4, 2002, Quebec City, Quebec, Canada
Clément M. Gosselin and Imme Ebert-Uphoff, editors

Design of a Parallel Wire-Driven Manipulator for Wind Tunnels

PASCAL LAFOURCADE
DCSD ONERA-CERT
B.P. 4025, 2 avenue Edouard Belin,
31055 Toulouse cedex 4, France
pascal.lafourcade@cert.fr

MICHEL LLIBRE
DCSD ONERA-CERT
B.P. 4025, 2 avenue Edouard Belin,
31055 Toulouse cedex 4, France
michel.llibre@cert.fr

CLAUDE REBOULET
DCSD ONERA-CERT
B.P. 4025, 2 avenue Edouard Belin,
31055 Toulouse cedex 4, France
claude.reboulet@cert.fr

Abstract: *This paper deals with the design of a 6 d-o-f wire-driven manipulator. In the introduction we present its application field, why we chose a wire-driven manipulator and a short state of the art. In the second part we develop a geometrical approach for the architecture design. In the third part, we present a kinematic and dynamic model of the manipulator which is used to compute the manipulator workspace and we introduce the control principles.*

1 INTRODUCTION

1.1 SACSO goals

Our research on wire-driven manipulators takes place within the SACSO[1] project. This project deals with the study of aircraft behavior and more precisely with the identification of its aerodynamic coefficients. The study of aircraft flight has been a big part of ONERA research since its creation.

The free flight simulation concept in wind tunnels through an active suspension comes from the most recent robotic researches outcomes, and more specifically from the improvement in parallel manipulator and force control. Our experience in this domain at ONERA leads us to the conception of an active suspension to simulate free flight.

This suspension sustains a model-scale in a wind tunnel and has to reproduce propulsion forces and to create virtual mass and inertia in order to respect the similitude coefficients.

The suspension must have displacement capabilities for the model-scale installation and for standard tests purposes. It must have a high bandwidth force control to simulate the propulsion effects and to confer an artificial inertia to the model-scale. These two control capabilities have to be ensured along 6 d.o.f. to allow free flight. The suspension should not disturb the streamline flow and must be implemented in existing wind tunnels with little modification. Series type robot structures are too heavy and cumbersome to cope with theses constraints. For these reasons we choose a wire-driven suspension manipulator.

1.2 Wire-driven manipulator description

Wire-driven (or tendon-driven) mechanisms are mechanisms using wires (or tendons) to transmit effort or motion (figure 1[2]). We are not interested here in those using wires in addition to rigid links , which are generally serial type manipulators. The problems (especially the kinematics ones) they raise are quite different [1]. We are interested in the ones using exclusively wires. They are parallel mechanisms [2] [3]. Verhoven and Hiller speak about "Tendon-driven Stewart Platform" [4].

A first kind of application for wire-driven manipulators is robot cranes, e. g. in shipbuilding [5] [6]. These manipulators can be classified in the Incompletely Restrained Positioning Mechanism (IRPM) class. The number of wires is equal to the number of d.o.f.. A second kind of application is very fast manipulators. The FALCON-7 [7] and the WARP manipulator [8] belong to this application field. They can be classified in the Completely Restrained Positioning Mechanism (CRPM) class when

[1] Suspension ACtive pour SOufflerie

[2] these two figures come from Verhoeven web site

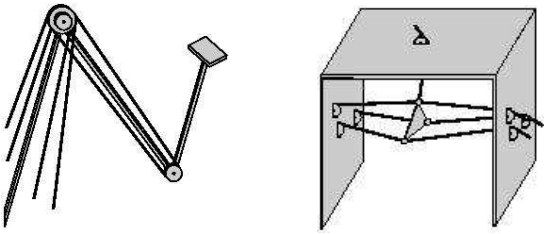

(a) Example of a tendon-driven serial manipulator

(b) Example of a tendon-driven Stewart Platform

Figure 1: The two types of wire-driven mechanisms

they use 7 wires or in the Redundantly Restrained Positioning Mechanism (RRPM) class when they use 8 wires [9] and more. With CRPM or RRPM, an another type of application is the virtual reality like virtual sport training [10].

2 GEOMETRICAL CONCEPTION OF A WIRE-DRIVEN MANIPULATOR

2.1 Introducing the method

We propose a geometrical approach to design wire-driven manipulators which use the designer experience. Although it is a very old method, it is the quickest one to obtain a preliminary architecture. In spite of those advantages, this approach does not seem to be used in this domain.

The fundamental principle of this approach lies in the fact that a tendon can only exert traction forces along its own direction.

In the following paragraphs we use this approach to design a manipulator whose workspace (according to Verhoeven definition of workspace [11]) is compatible with the application requirements.

We must keep in mind that the function of the wire driven manipulator is to sustain an aircraft model-scale in a wind tunnel. That implies that motion and clutter volumes are cylindrical.

In a first phase we design a 7-wire manipulator, but to increase substantially the workspace, we design, in a second phase, a 9-wire manipulator.

2.2 Application to the design of the parallel wire-driven manipulator SACSO-7

This first manipulator is a 7-wire parallel wire-driven mechanism. The mobile part is driven by seven wires anchored on it. They come from actuators and pass through pulleys, both are fixed on the stationary base frame.

Fixing the position and the orientation of a solid in a 3D coordinate frame requires the control of only three of its points which could be the wire anchorages on the mobile part. In our architecture, these three anchorages are the apexes of an isosceles triangle which is materialized by a T-cross (figure 2). The longitudinal rod controls the pitch and the course while the lateral one controls the roll[3]. Logically, the same symmetrical plans are taken for the aircraft model-scale and the suspension (particularly (O_x, O_z)). It gives the T-cross orientation in regards with the model-scale, and by extension with the wind tunnel and so with the stationary base frame. Positionning seven wires symmetrically on a T-cross at three points for a working solution does not offer a lot of possibilities. It is clear that four wires and more linked at the same anchorage point do not give more control than three. So, there are two possibilities : 1-3-3 and 3-2-2 (figure 2). Solution 1-3-3 does not work because an arbitrary torque around O_y cannot be made (torque can be made in only one way). It consequently leaves only one possibility: 3-2-2.

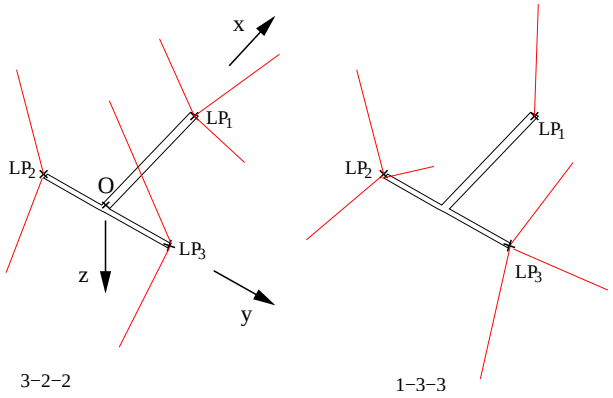

Figure 2: Only two possibilities for 7 wires linked on three points with no more than 3 wires on the same point

Wires linked on LP1 will be called front wires and those linked on LP2 and LP3 will be called back wires.

Now, pulleys locations on the stationary base frame have to be chosen. Tacpoint between wires and pulleys are approximated to fixed point. A wire can only pull. So, with a planar reasoning, LP1 must stay in the triangle described by the three front wire tacpoints on the base frame. To have the bigger surface, an equilateral triangle is chosen. In the case of the back wires, which transmit roll motion or effort (around O_x) the problem is different. Planar (plan (O_y, O_z)) reasoning and sketches are used to design and to study different solutions.

There are four back wires. The evident solution is a square (always the maximal surface for a quadrilateral in a circle). Planar translation motions are limited in this square. Figure 3 shows roll motion abilities. With this particular pose, wires 2 and 3 are aligned and only wires 1 and 4 can exert torques, and only in the negative direction. It is a singular pose, and if the roll increases beyond that limit, all wires would generate torques in negative direction. There would be one d.o.f. left.

[3] since the application is in the field of aeronautics, we use aeronautical references and angles

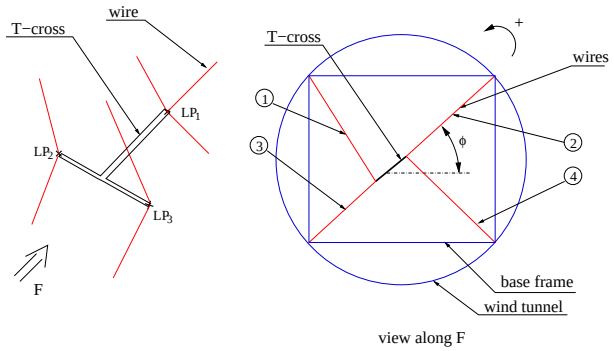

Figure 3: The square solution

Another solution, increasing roll abilities, is the diamond as shown on figure 4. Sketches show that the loss in O_Y motion abilities is greater than the gain in roll abilities. The maximum motion along O_Y is reached when wires 1 and 3 (or 2 and 4 as shown on the sketch) are aligned.

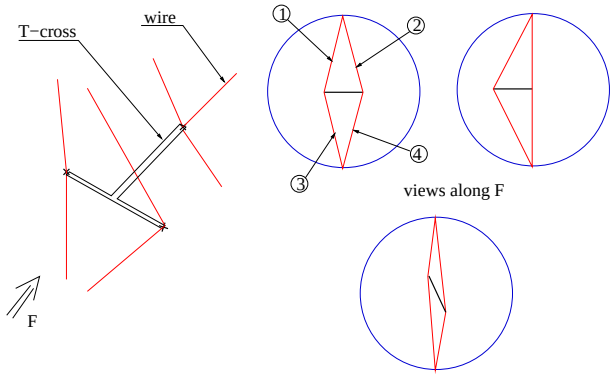

Figure 4: The diamond solution

To get the roll abilities of the diamond solution without its disadvantages, the principle of a “pendulum” is kept and an anchorage point is added. To respect symmetry, the point is added on the longitudinal rod. Tacpoints form an equilateral triangle on the stationary base frame. So the roll abilities are the same as those with the diamond solution and the planar motion surface is the triangle.

Pendulum solution is chosen, particularly for its roll abilities. As the (O_X, O_Z) reflective symmetry must be respected, there are two possibilities to merge the front wires solution and the back wires solution. They are shown on figure 6(a) and 6(b).

Starting with given roll and translation along O_Y specifications, we study geometrically the other motions to obtain the complete workspace. Top views and lateral views figures permit to study abilities in pitch motion (around O_y) and course motion (around O_z). It is not difficult to detect singular angular pose if the T-cross stays at the center of the base frame like it is shown

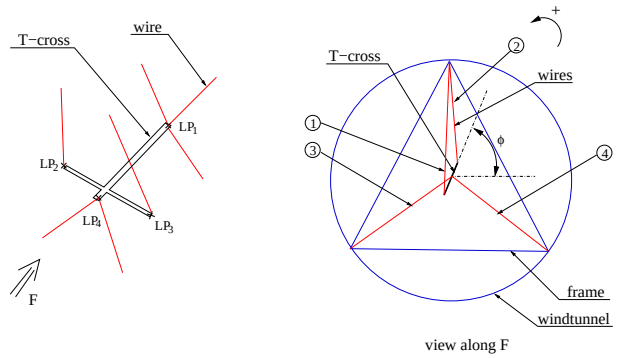

Figure 5: The pendulum solution

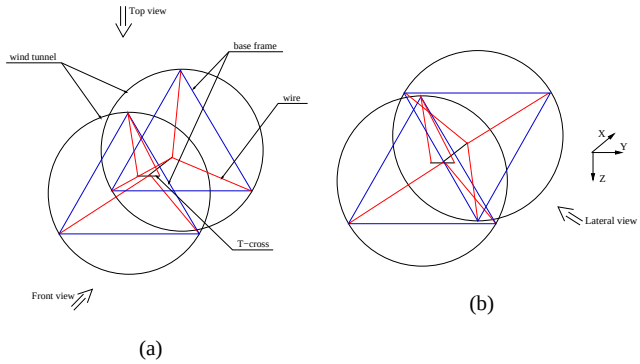

Figure 6: Two possibilities for SACSO-7

on figures 7(a) and 7(b). We can see that angular abilities decrease with the length of the stationary base frame, contrary to translations abilities along O_X which increase.

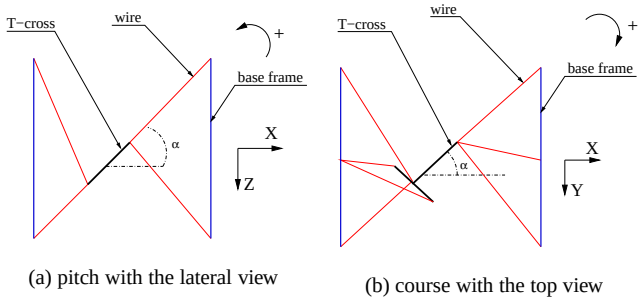

(a) pitch with the lateral view

(b) course with the top view

Figure 7: Singular angle pose at the center of the base frame

If the T-cross is not at the center, the analysis is more complex. For example, in figure 8(a), two wires (not really, some are coincident on the sketch) generate positive torque (around O_y), and two other ones generate negative torque; this pose is inside the workspace. On figure 8(c), all wires generate negative torque. This pose is outside the workspace. On figure 8(b),

one wire generate positive torque and the three others generate negative torque. It could works, but certainly badly, and T rod goes through a singular pose to reach it. It is certainly out of the workspace.

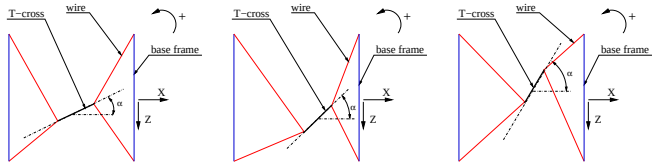

(a) case one, it works (b) case two, it should not work (c) case three, it does not work

Figure 8: graphical study of pitch limitation, mobile part not at the center of the base frame

Same type of analysis can be made for course abilities.

2.3 Operational workspace

Finally, with some geometrical considerations, we have got an idea of the workspace of the robot. In the two cases (6(a) & 6(b)) the 3D workspace in translation is not smooth enough. It is dangerous to ride near singularity and corner. Actually, the manipulator is not commanded in position and the aircraft model-scale behavior is not well monitored. So we decide to limit the workspace to a cylindrical base cylinder, like it is showed in figure 9. It is the same cylinder in both cases.

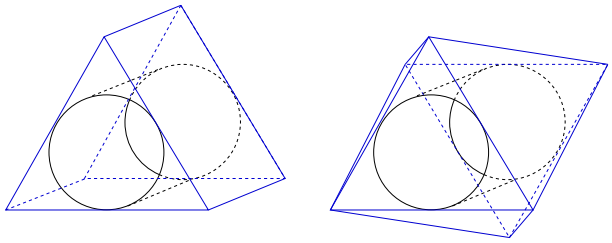

Figure 9: workspace is restricted to a cylinder

The problem is that this volume (and so the workspace) is too little. It is directly connected to the form described by the tacpoints on the stationary base frame. The surface of the circle inscribed in a square, itself inscribed in a circle, is twice bigger than the surface of the circle inscribed in a triangle, itself inscribed in the same external circle (figure 10). Next, we propose solutions with nine wires whose tacpoints describe two squares.

2.4 An evolution : SACSO-9

To design this RRPM[4] manipulator, we have kept the same concept as SACSO-7, with two square frames instead of triangular

[4]Redundantly Restrained Positioning Mechanism

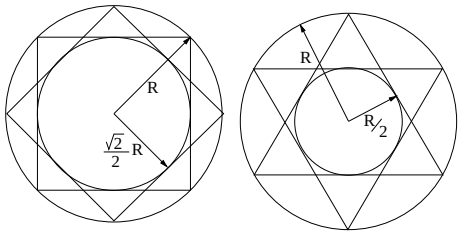

Figure 10: comparison of surfaces inside square or triangle

frames. So, we have kept the same rod, and have just added one front wire and two back wires.

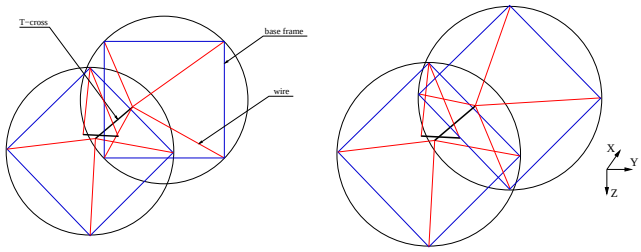

(a) solution 1 (b) solution 2

Figure 11: Two solutions for the 9-wire manipulator

Figure 11 shows two solutions : the one presented on figure 11(b) is not acceptable because there is a contact between front wires and wings. It lets solution figure 11(a). An OpenGL based visualization was developed. Figure 12 shows two view of the whole suspension.

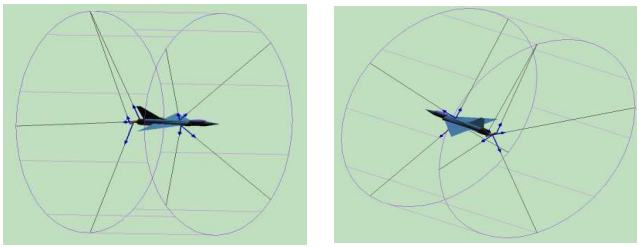

(a) 3/4 front view (b) 3/4 back view

Figure 12: The manipulator with the model-scale

The same design principle conducts almost to the same rotational motion workspace. Its 3d workspace in translation are shown on figure 13. We again limit this workspace to the inside of the cylinder.

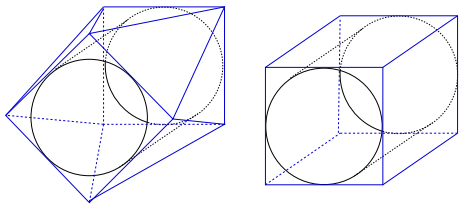

Figure 13: simplified figure of SACSO-9 displacement workspace

2.5 Conclusion on the method

The geometrical approach presented in this chapter gives just some ways and ideas for a first design of the manipulator. Of course, to obtain the complete workspace, it is necessary to use numerical method : including the study of the Jacobian and the study of wires tensions. In the following, we expose our modelisation and we explain our method to calculate wire tension and which is then applied to SACSO-7 and SACSO-9.

3 MODELISATION OF THE WIRE-DRIVEN MANIPULATORS

As shown on figure 14, let us note A_i the first contact points between wire and pulley on the fixed structure, B_i the anchoring points with the support(ed) model, $\vec{L}_i = \overrightarrow{B_iA_i}$, $l_i = \left\|\vec{L}_i\right\|$, $\vec{u}_i = \frac{1}{l_i}\vec{L}_i$ and t_i the tension in the cable i which exerts a force $\vec{T}_i = t_i\vec{u}_i$ on the support. G is the center of gravity of the scale model and $\vec{r}_i = \overrightarrow{GBi}$.

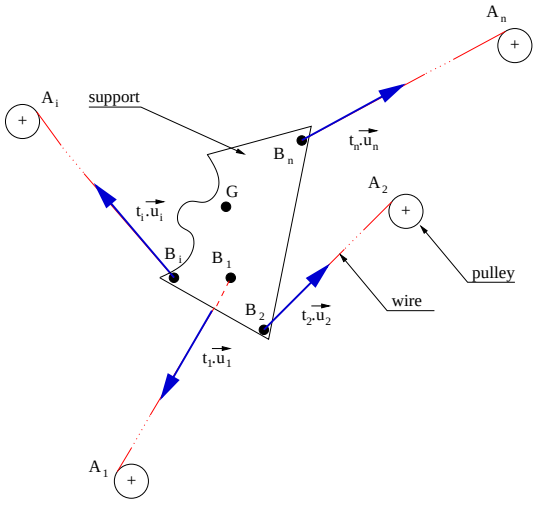

Figure 14: Sketch of a general parallel wire-driven mechanism

As far as notation is concerned, $\vec{V}$ is used for three components vectors like forces, torques, velocities, and $\mathbf{V}$ for other vectors (six components vectors) and matrices.

3.1 Kinematic and Static

We have $\dot{l}_i = \vec{u}_i \cdot \vec{V}_{B_i}$ and $\vec{V}_{B_i} = \vec{V}_G + \vec{\Omega} \times \vec{r}_i$ where $\vec{V}_G$ and $\vec{\Omega}$ are respectively the support translation and rotation velocities, so $\dot{l}_i = \vec{u}_i \cdot \vec{V}_G + \vec{u}_i \cdot \left(\vec{\Omega} \times \vec{r}_i\right)$. Permuting the triple scalar product yields to the well known form of the parallel manipulator Jacobian :

$$\dot{\mathbf{l}} = \mathbf{P}^{\mathsf{T}}\mathbf{W} \tag{1}$$

where $\dot{\mathbf{l}}$ is the l_i-component vector, $\mathbf{W}$ is the 6-component vector $\begin{pmatrix} \vec{V}_G \\ \vec{\Omega} \end{pmatrix}$ and $\mathbf{P}$ is given by :

$$\mathbf{P} = \begin{pmatrix} \vec{u}_1 & \cdots & \vec{u}_n \\ \vec{r}_1 \times \vec{u}_1 & \cdots & \vec{r}_n \times \vec{u}_n \end{pmatrix}$$

Let us note $\overrightarrow{F}$ the resultant force and $\overrightarrow{M_G}$ the resulting moment in G of the $t_i\vec{u}_i$. We have $\overrightarrow{F} = \sum_i t_i\vec{u}_i$ and $\overrightarrow{M_G} = \sum_i \vec{r}_i \times t_i\vec{u}_i$, so :

$$\mathbf{F} = \mathbf{PT} \tag{2}$$

where $\mathbf{T}$ is the t_i components vector and $\mathbf{F}$ is the 6 components vector $\begin{pmatrix} \overrightarrow{F} \\ \overrightarrow{M_G} \end{pmatrix}$.

Let us note $\mathbf{T_{eff}} = \mathbf{P}^{+}\mathbf{F}$ the minimal norm solution of (2), where $\mathbf{P}^{+}$ is the Moore-Penrose[5] inverse of $\mathbf{P}$, and $\mathbf{T_{nul}}$ a vector belonging to the null space $\mathcal{N}(\mathbf{P})$ of $\mathbf{P}$.

We can write the general solution in the form :

$$\mathbf{T} = \mathbf{T_{eff}} + \mathbf{T_{nul}} \tag{3}$$

Note that (1), (2), (3) and $\mathbf{P}.\mathbf{T_{nul}} = 0$ imply :

$$\mathbf{W} = \left(\mathbf{PP}^{\mathsf{T}}\right)^{-1}\mathbf{P}\dot{\mathbf{l}} \tag{4}$$

The model-scale speeds are obtained according to the wires speeds by the least squares inverse.

To maintain a minimal tension in the wires, we propose the following expression for $\mathbf{T_{nul}}$: $\mathbf{T_{nul}} = (\mathbf{I}_{n\times n} - \mathbf{P}^{+}\mathbf{P})\mathbf{T_{des}}$ where $\mathbf{T_{des}}$ is a desired value of $\mathbf{T}$ which is used as a control variable.

3.2 Dynamics

The dynamic model of the motors is written as :

$$\mathbf{T}_m + \mathbf{T}_f - \mathbf{T} = \mathbf{m}_m\ddot{\mathbf{l}} \tag{5}$$

where $\mathbf{T}_m$ is the vector of the driving forces, $\mathbf{T}_f$ is the vector of the friction forces and $\mathbf{m}_m$ is a diagonal matrix of motors inertias. The dynamic model of the scale-model is written as :

$$\frac{d}{dt}(\mathbf{A}_G\mathbf{W}) = \mathbf{F}_G + \mathbf{F}_A + \mathbf{F} \tag{6}$$

[5] $\mathbf{P}^{+} = \mathbf{P}^{\mathsf{T}}(\mathbf{PP}^{\mathsf{T}})^{-1}$

where $\mathbf{A}_G = \begin{pmatrix} m_A\mathbf{I}_{3\times3} & \mathbf{0}_{3\times3} \\ \mathbf{0}_{3\times3} & \mathbf{J}_G \end{pmatrix}$ is the matrix of inertia of the model-scale at its center of gravity, $\mathbf{F}_G = \begin{pmatrix} m_A\vec{g} \\ 0 \end{pmatrix}$ the torque of the forces of gravity, $\mathbf{F}_A$ the torque of the aerodynamic forces and $\mathbf{F}$ the torque exerted by the support. These two equations are connected by the relations (1) and (2).

The inertia of the engines seen by the model is obtained immediately by expressing the kinetic energy of the whole system according to the speeds model : $e = \frac{1}{2}\left(\mathbf{W}^\mathsf{T}\mathbf{A}_G\mathbf{W} + \dot{\mathbf{l}}^\mathsf{T}\mathbf{m}_m\dot{\mathbf{l}}\right)$. By using relation (1) we obtain :

$$\mathbf{A}_{Gtot} = \mathbf{A}_G + \mathbf{P}\mathbf{m}_m\mathbf{P}^\mathsf{T}$$

But to make the synthesis of the driving forces control correctors, we must estimate the inertia of the scale model seen by the motors. For that, we use relation (4). So :

$$\mathbf{m}_{mtot} = \mathbf{m}_m + \mathbf{P}^\mathsf{T}\left(\mathbf{P}\mathbf{P}^\mathsf{T}\right)^{-1}\mathbf{A}_G\left(\mathbf{P}\mathbf{P}^\mathsf{T}\right)^{-1}\mathbf{P}$$

4 WORKSPACE EXPLORATION WITH WIRE TENSIONS

4.1 Wire tension calculus

In order to get a satisfactory behavior of the mechanism and the actuators, we chose a desired tension in wires $\mathbf{T}_{des}$. For preliminary studies, the scheme to calculate tension is very simple. It consists in minimizing $\|\mathbf{T} - \mathbf{T_{des}}\|^2$ while respecting (2) and $min(\mathbf{T}) > t_{min}$. The proposed algorithm is :

Evaluating position
calculating $\mathbf{P}$
$\mathbf{T_{eff}} = \mathbf{P}^{+}\mathbf{F}$
$\mathbf{T_{nul}} = (\mathbf{I}_{n\times n} - \mathbf{P}^{+}\mathbf{P})\mathbf{T}_{des}$
$\mathbf{T} = \mathbf{T} + \mathbf{T}_{null}$
if $min(\mathbf{T}) < t_{min}$ then
  $\mathbf{T} = \mathbf{T} + \lambda\mathbf{T}_{null}$
  with $\lambda \mid min(\mathbf{T}) = t_{min}$
end if

4.2 Workspace capacities in displacement along O_Y and roll

Because of the complexity of the worspace (3 d.o.f. in displacement and 3 d.o.f. in orientation), it is quite difficult to represent it (so the sketches used in subsection 2.2). The calculus of the wire tensions for a given load will help us geting a more precise definition of this workspace.

For example, we studied in subsection 2.2 three types of 7-wires manipulators. We saw with a graphical approach that diamond and pendulum are better than square for roll motions, but diamond is quite bad in displacement along O_Y. We proposed section 2.4 the 9-wires manipulator SACSO-9, equal in roll capacities with pendulum but better in displacement along O_Y.

To confirm those feelings, we have calculated wires tensions during displacement along O_Y with other pose parameters equal to zero, and wires tensions during roll rotation with another parameters equal to zero[6]. The calculation scheme used is the one presented in subsection 4.1, with $t_{min} = 20N$ and $\mathbf{T}_{des} = \begin{pmatrix} t_{des} \\ \vdots \\ t_{des} \end{pmatrix}$, $t_{des} = 100N$. The load is equal to the weight of the model-scale, $50N$ and the drag, $10N$. The maximal tension in wires is $240N$. Dimensions of the T-cross are $0.6m \times 0.16m$ and the dimensions of the stationary base frame are $\phi = 3m \times L = 1.5m$.

Wires tensions along O_Y displacement are shown on figures 15 to 18, and wires tensions along roll rotation on figures 19 to 22. Lines with little circles[7] are for front wires and lines with little triangles[8] are for back wires.

Figures 15 to 18 confirm that roll abilities of the square solution ($\simeq \pm 45^o$) is smaller than roll abilities of the other solution ($\simeq \pm 90^o$). For tranlation abilities along O_Y , figures 19 to 22 show there are smaller in case of square solution, compared to the case of SACSO-9, despite the fact that back wires are linked on a similar square in both case. This is because front wires are linked on a triangle in one case and on a square in the other case.

5 CONCLUSION AND PERSPECTIVES

The work done in the frame of the SACSO project will lead to the build-up of a prototype of the wire-driven manipulator by the end of 2002. We already tested the control principles on a one degree of freedom setup, in which both tendons were force controlled (figure 23). We are now working, in a theoretical way, on an increase of the workspace of the manipulator through an optimization process and on the management of the multiple redundancies.

References

[1] Y. J. Ou and L.-W. Tsai. Theory of isotropic transmission for tendon-driven manipulators. In *Robotics: Kinematics, Dynamics and Control*, pages 53–61, Minneapolis, USA, 1994. ASME.

[2] A. Ming and T. Higuchi. Study on multiple degree-of-freedom positioning mechanism using wire-concept, design and control (part 1). *Intl. J. of the Japan Society for Precision*, 28(2):1331–138, juin 1994.

[3] A. Ming and T. Higuchi. Study on multiple degree-of-freedom positioning mechanism using wire-concept, part 2, development of a planar completely restrained position-

[6] the zero is where the middle of the T-cross is at the middle of the cylinder
[7] red
[8] green

ing mechanism. *Intl. J. of the Japan Society for Precision*, 28(3):235–242, septembre 1994.

[4] R. Verhoeven and M. Hiller. Estimating the controlable workspace of tendon-based stewart platforms. In *Proc. 7th Int. Symposium on Advances in Robot Kinematics"*, pages 277–284, 2000.

[5] J. Albus, R. Bostelman, and N. Dagalakis. The nist robocrane. *J. of Robotic Systems*, 1993.

[6] N. G. Dagalakis, J. S. Albus, B.-L. Wang, J. Unger, and J. D. Lee. Stiffness study of a parallel link robot crane for shipbuilding applications. *ASME Journal of Offshore Mechanics and Arctic Engineering*, pages 183–193, 1989.

[7] S. Kawamura, H. Kino, and C. Won. Hight-speed manipulation by using parallel wire-driven robots. *Robotica*, 18:13–21, 2000.

[8] K. Maeda, S. Tadokoro, T. Takamori, M. Hiller, and R. Verhoeven. On design of a redundant wire-driven parallel robot warp manipulator. In *International Conference on Robotics & Automation*, pages 895–900. IEEE, Mai 1999.

[9] S. Tadokoro, S. Nishioka, T. Takamori, and K. Maeda. On fundamental design of wire configurations of wire driven parallel manipulators with redundancy. In *Proceedings of Japan-U.S.A. Symposium on Flexible Automation*, volume 1, pages 151–158, 1996. Boston, U.S.A.

[10] T. Morizono, K. Kurahashi, and S. Kawamura. Realization of a virtual sports training system with parallel wire mechanism. In *Proc. of the 1997 IEEE International Conference on Robotics and Automation*, pages 3025–3030, Albuquerque, New Mexico, April 1997. IEEE.

[11] R. Verhoeven, M. Hiller, and S. Tadokoro. Worspace, stiffness, singularities and classification of tendon-driven stewart platforms. In *Proc. 6th Int. Symposium on Advances in Robot Kinematics*, pages 105–114, Strobl/Salzburg, Austria, 29 juin-4 juillet 1998.

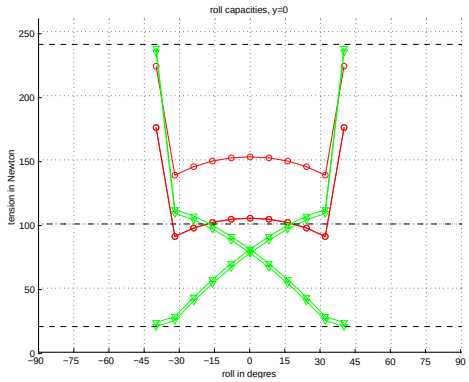

Figure 15: Square solution (figure 3). It is seen that roll max is under 45^o

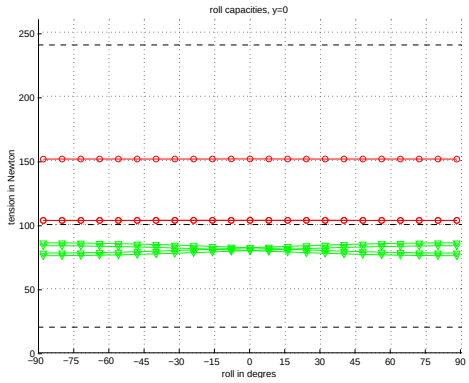

Figure 16: Diamond solution (figure 4). With the chosen load (no torque load), almost no limitation in roll

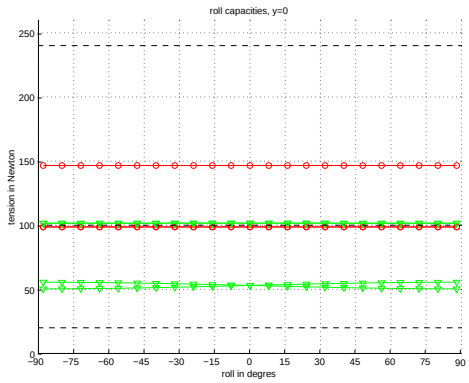

Figure 17: Pendulum solution (figure 5), same abilities than diamond solution

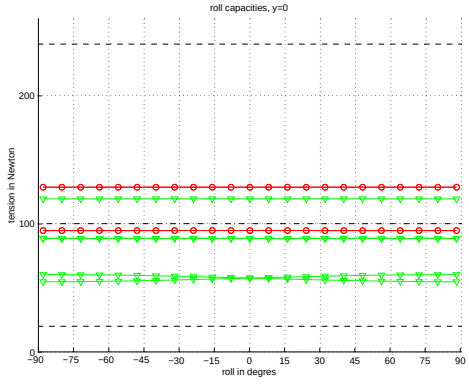

Figure 18: SACSO-9 (figure 11(a)) same abilities than diamond solution

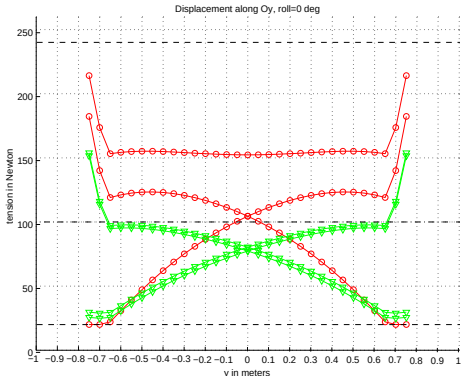

Figure 19: Square solution (figure 3). $y_{max} \simeq 0.75m$

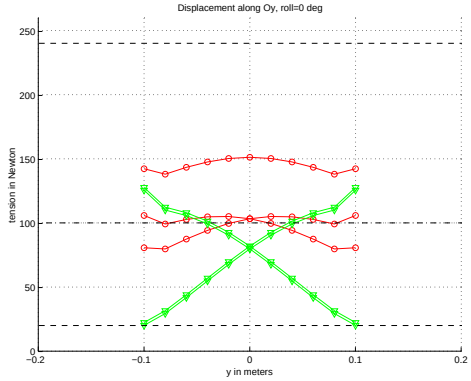

Figure 20: Diamond solution (figure 4). $y_{max} \simeq 0.1m \ < T - cross\ width$

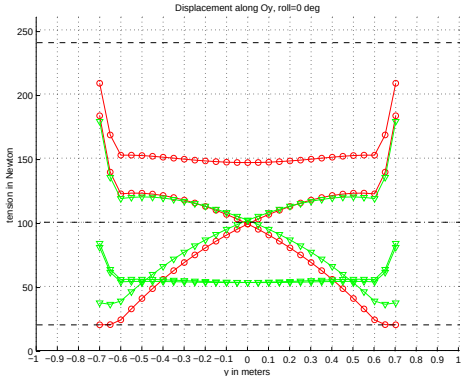

Figure 21: Pendulum solution (figure 5). $y_{max} \simeq 0.7m$

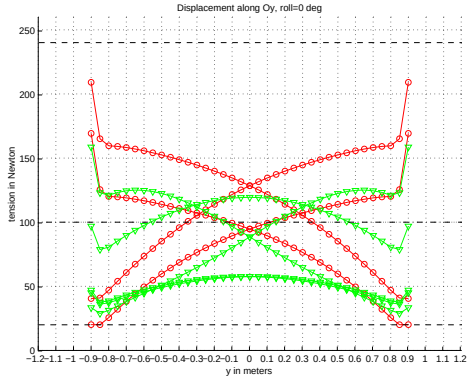

Figure 22: SACSO-9 (figure 11(a)). $y_{max} \simeq 0.9m$

Figure 23: One d.o.f. testing ground for control principle